Supplementary Information

Sub-100 fs mode-locked fiber deep-red laser for multicolor two-photon microscopy

Jinhai Zou[a, b, †], Hongsen He[a, †], Luming Song[a, c], Lu Huang[a], Jingbin Lan[a], Lan Lan[a], Tingting Chen[a], Cihang Kong[d], Zhipei Sun[e], Zhengqian Luo[a, c, *]

[a]Fujian Key Laboratory of Ultrafast Laser Technology and Applications, School of Electronic Science and Engineering, Xiamen University, Xiamen 361005, China.

[b]College of Advanced Interdisciplinary Studies, National University of Defense Technology, Changsha 410073, China.

[c]Shenzhen Research Institution of Xiamen University, Shenzhen, China.

[d]Institute for Translational Brain Research, MOE Frontiers Center for Brain Science, Fudan University, Shanghai 200032, China.

[e]Department of Micro- and Nanosciences, Aalto University, FI-02150 Espoo, Finland.

[*]Corresponding author: zqluo@xmu.edu.cn.

1. Parameters calculation

The formula for the nonlinear coefficient (γ) is expressed as follows:

$$\gamma = 2\pi n_2/\lambda A_{\text{eff}} \quad \text{(S1)}$$

Here, n_2 denotes the nonlinear refractive index, λ and A_{eff} represent the laser wavelength and the effective mode field area of the fiber, respectively. The nonlinear coefficient (γ) of DC Pr^{3+}: ZBLAN fiber at 717 nm can be calculated as 0.0048 W^{-1} m^{-1}. For this calculation, we utilized a nonlinear refractive index (n_2) of 2.1×10^{-20} m^2 W^{-1} and an effective mode field area (A_{eff}) of 37.75 μm^2.

In addition, we numerically calculated the group velocity dispersion coefficient (β_2) of the DC Pr^{3+}: ZBLAN fiber, as plotted in Fig. S1. The β_2 value is 0.0626 ps^2 m^{-1} at 717 nm.

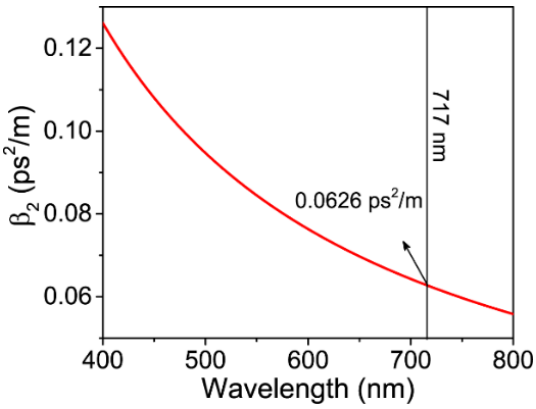

Fig. S1 Group velocity dispersion coefficient (β_2) of the DC Pr^{3+}: ZBLAN fiber.

2. Numerical model

The numerical simulation model was constructed based on our experimental setup (*i.e.*, Fig. 1(a)). The parameters utilized in the simulation, such as γ, β_2 of gain fiber, and β_2 of TGs, are elaborated in the Experimental Setup and Operation Principle. The pulse propagation in the deep-red fiber laser is governed by the Ginzburg-Landau equation (GLE), which incorporates key physical effects like group velocity dispersion (GVD), self-phase modulation, and gain saturation with finite bandwidth. The GLE is formulated as follow[24]:

$$\frac{\partial A(z,t)}{\partial z} = \frac{g}{2}A(z,t) - \frac{i\beta_2}{2}\frac{\partial^2 A(z,t)}{\partial t^2} + i\gamma|A(z,t)|^2 A(z,t) + \frac{g}{2\Omega^2}\frac{\partial^2 A(z,t)}{\partial t^2} \quad (1)$$

Here, $A(z,t)$ is the electric field envelope, t and z stand for the pulse local time and propagation distance, Ω and g denote the gain bandwidth and gain function of the gain fiber. Generally, the average power in the cavity should be considered when simulating the gain saturation of the gain fiber. The gain saturation effect is considered as follow:

$$g = \frac{g_0}{1 + P_{\mathrm{ave}}/P_{\mathrm{satg}}} \quad (2)$$

$$P_{\mathrm{ave}} = E_{\mathrm{P}}/T_{\mathrm{R}} \quad (3)$$

$$E_{\mathrm{P}} = \int_{-T_{\mathrm{R}}/2}^{T_{\mathrm{R}}/2} |A(z,t)|^2 dt \quad (4)$$

Here, g_0 is the small-signal gain coefficient, P_{satg} represents the saturation power of the gain fiber, P_{ave} is the intracavity average power, E_P refers to the single pulse energy, and T_{R} is the cavity roundtrip time, respectively. According to Equation (2), the gain of the laser is dependent on g_0 and P_{satg}. In our simulations, g_0 is fixed at 3.0 m^{-1}. In addition, the mode-locking element is the NPR that induces a saturable absorption (SA) effect. The transmission coefficient of an NPR mode-locker can be well described by the following equation[33]:

$$|T|^2 = \cos^2\ \theta_1 \cos^2\ \theta_2 + \sin^2\ \theta_1 \sin^2\ \theta_2 + \frac{1}{2}\sin\ 2\theta_1 \sin\ 2\theta_2 \cos\left(\Delta\varphi + \Delta\varphi'\right) \quad (5)$$

Here, the meanings of the corresponding parameters are given in the previous work[33]. According to Equation (5), the transmittance coefficient of the NPR mode-locker used in the simulation is obtained (see Fig. S2), and its modulation depth (ΔT) is approximately 44.5%. In the simulation, a Gaussian-shaped pulse with a pulse duration of 500 fs and a peak power of 1 W was used as the initial pulse to accelerate the convergence of the calculation to a mode-locking solution.

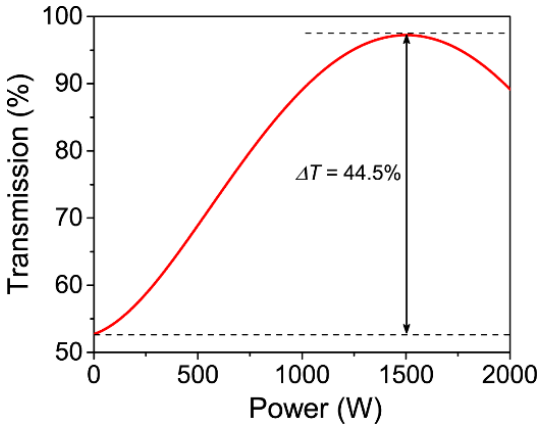

Fig. S2 Transmittance curve of NPR mode-locker used in our simulation.

3. Experimental results

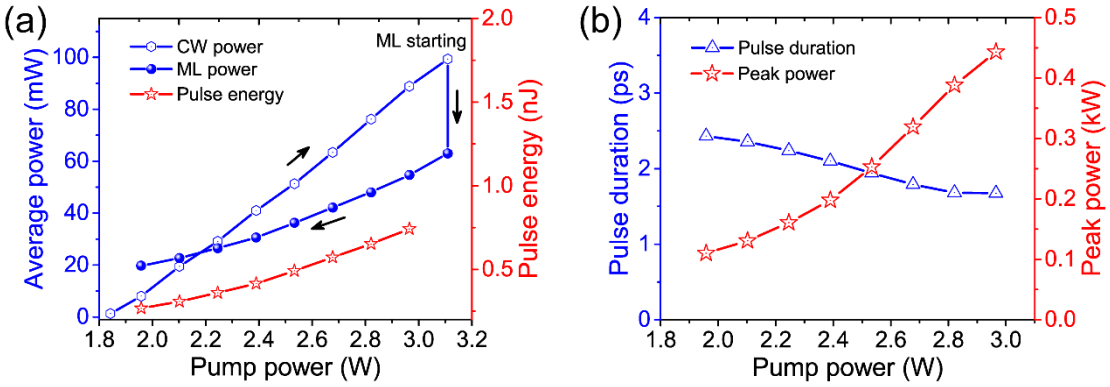

Fig. S3 Characteristics of deep-red MLFL extracted after PBS versus the pump power at the dispersion of +0.005 ps^2. (a) Average power and pulse energy; (b) Pulse duration and peak power.

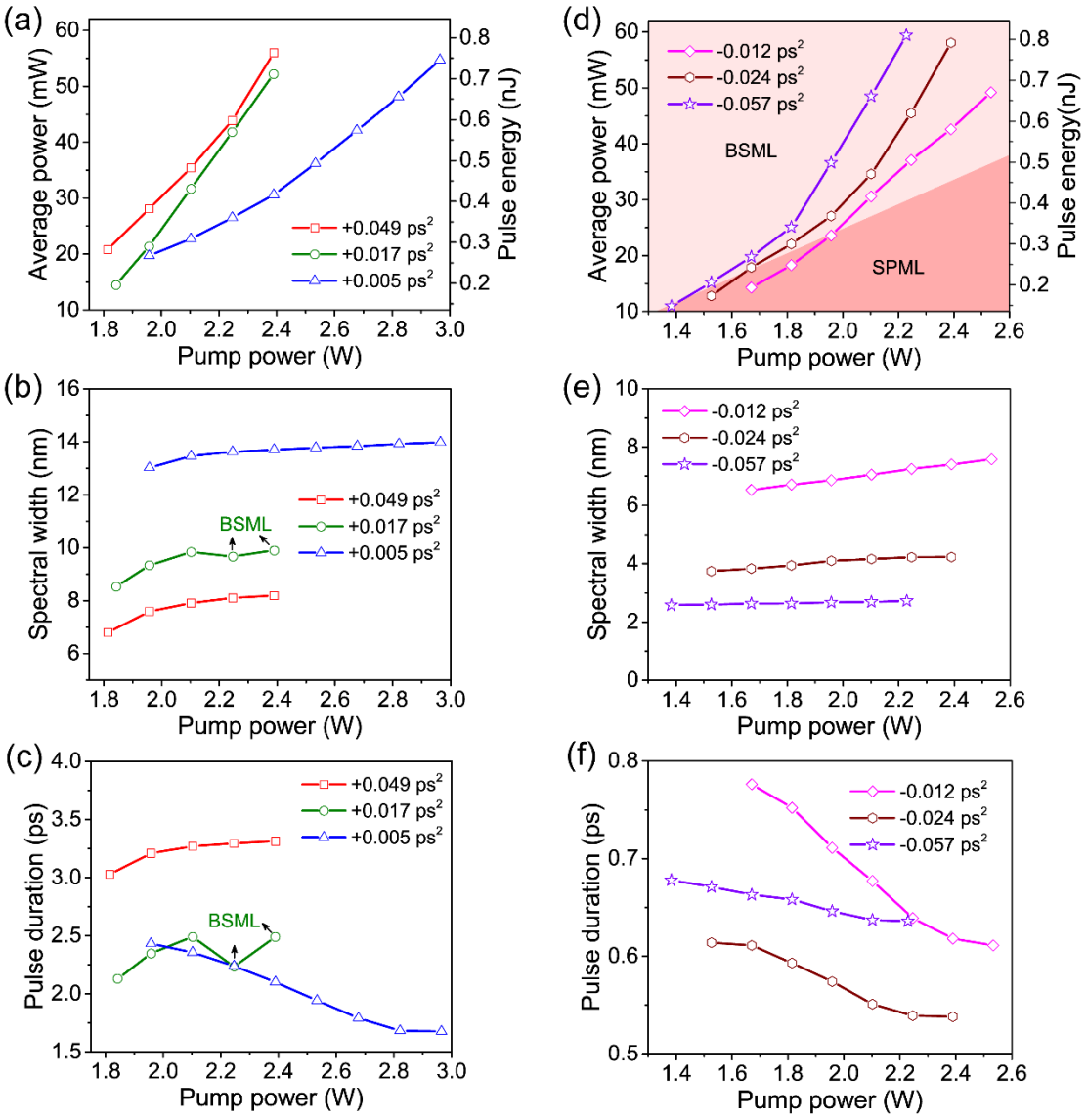

Fig. S4 Characteristics of deep-red MLFL extracted after PBS versus the pump power. (a-c) Output power, pulse energy, spectral bandwidth, and pulse duration under the dispersions of +0.049 ps^2, +0.017 ps^2, and +0.005 ps^2. (d-f) Output power, pulse energy, spectral bandwidth, and pulse duration under the dispersions of -0.012 ps^2, -0.024 ps^2, and -0.057 ps^2. BSML: bound-state soliton mode-locking.

Table S1 Performance of our deep-red MLFL with different dispersions.

Dispersion (ps^2)	P_p (mW)		Output from PBS					Output from DSM			
	ML-starting	SPML	Δλ (nm)	Δτ (fs)	TBP	P_o (mW)	P_{Peak} (W)	Δτ (fs)	TBP	P_o (mW)	P_{Peak} (W)
-0.057	2229	1383	2.58	678	1.02	11.0	222.0	281	0.42	6.1	297.1
-0.024	2390	1527	3.74	614	1.34	12.8	284.0	178	0.39	6.6	505.0
-0.012	2534	1670	6.53	728	2.77	14.3	267.2	142	0.54	7.5	718.6
0.005	3109	1958	13.0	2431	18.47	19.7	110.0	83	0.63	9.9	1618.8
0.017	2447	1958	9.33	2451	13.34	22.4	123.8	146	0.80	12.3	1141.6
0.049	2390	1814	6.79	2962	11.74	24.8	112.9	174	0.69	14.2	1100.7

From Table S1, it is evident that as the net dispersion varies from -0.057 ps^2 to +0.049 ps^2, the time-bandwidth products (TBPs) of the mode-locked pulses outputted from PBS exhibit a trend of change consistent with the spectral bandwidth of the mode-locking. Additionally, the dechirped pulses with negative net dispersions outputted from DSM are closer to the transmission limit pulse compared to those with normal net dispersions.

4. Simulation results

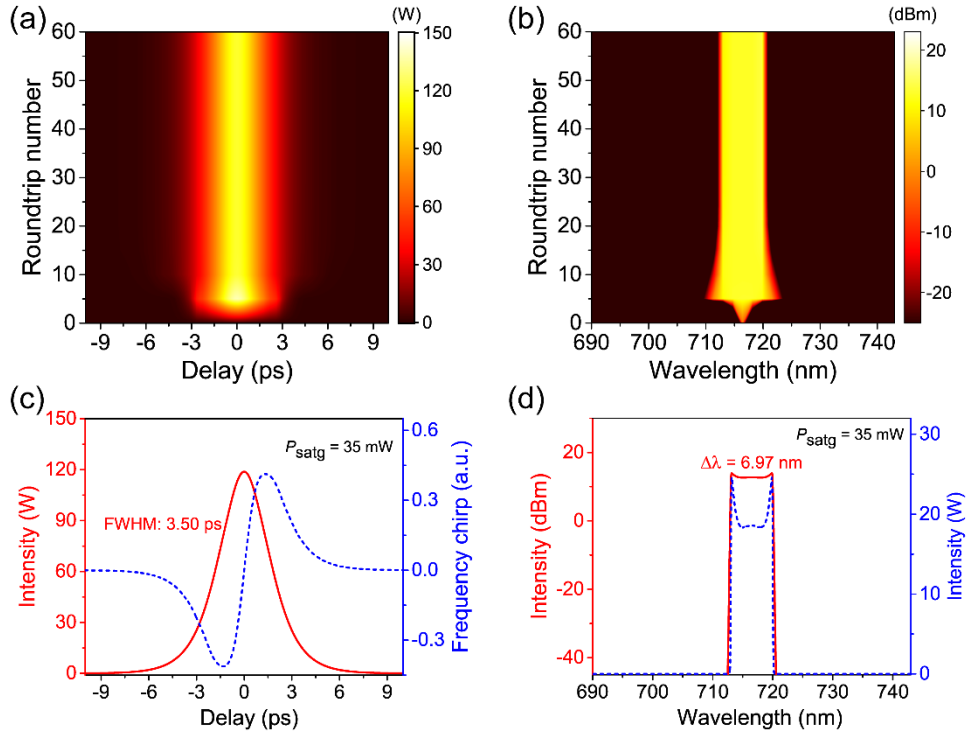

Fig. S5 Simulation results of deep-red MLFL under the net dispersion of +0.049 ps^2. (a) Pulse evolution; (b) Spectrum evolution; (c) Pulse temporal profile (solid) and frequency chirp (dashed); (d) Spectra on a logarithmic scale (solid) and on a linear scale (dashed).

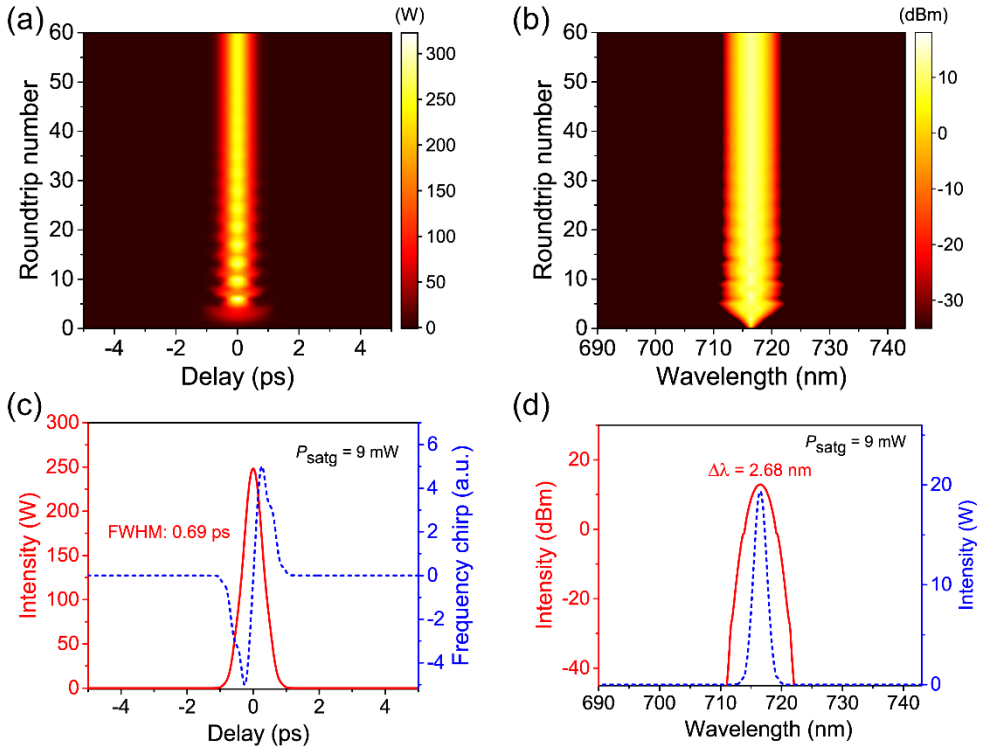

Fig. S6 Simulation results of deep-red MLFL under the net dispersion of -0.057 ps^2. (a) Pulse evolution; (b) Spectrum evolution; (c) Pulse temporal profile (solid) and frequency chirp (dashed); (d) Spectra on a logarithmic (solid) or linear (dashed) scale.

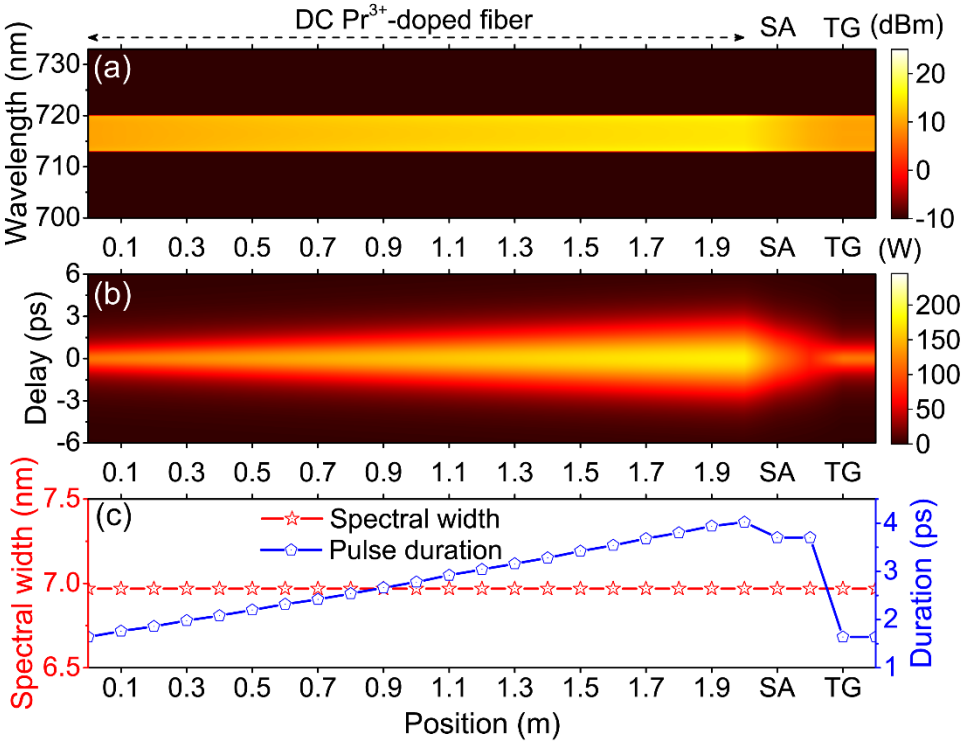

Fig. S7 Simulation performance of intracavity pulse dynamics at the net dispersion of +0.049 ps^2. (a) Spectrum evolution; (b) Pulse evolution; (c) Spectral bandwidth and pulse duration.

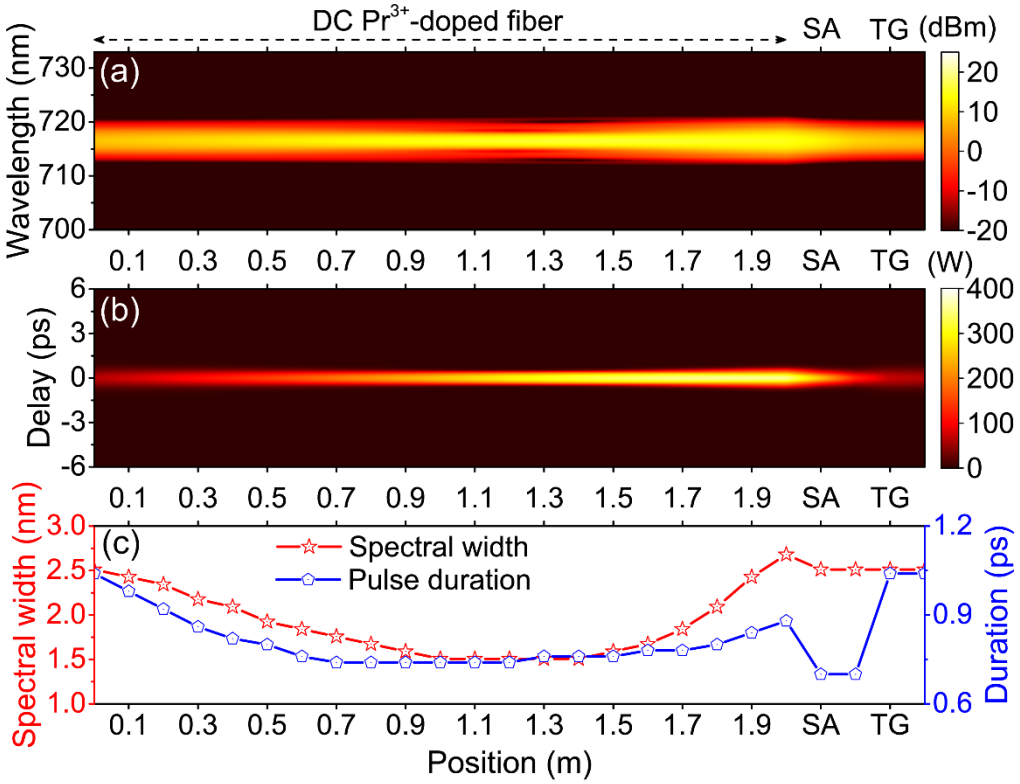

Fig. S8 Simulation performance of intracavity pulse dynamics at the net dispersion of -0.057 ps^2. (a) Spectrum evolution; (b) Pulse evolution; (c) Spectral bandwidth and pulse duration.

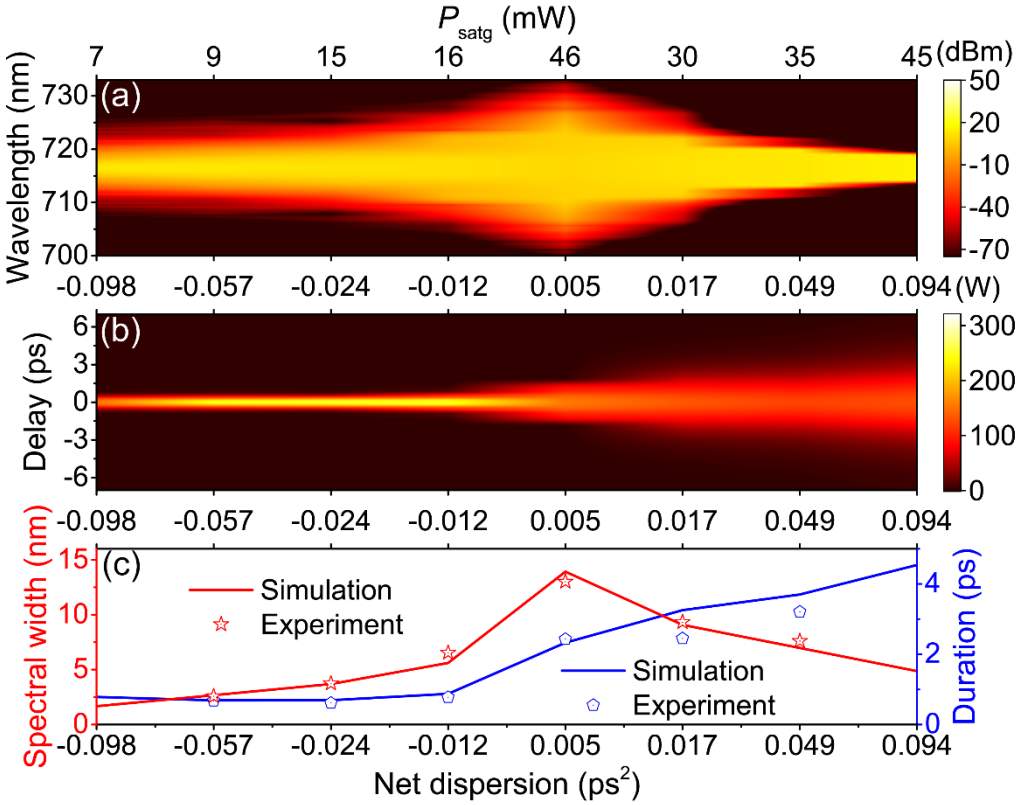

Fig. S9 Simulation performance of MLFL with different net dispersions. (a) Spectrum evolution; (b) Pulse evolution; (c) Spectral bandwidth and pulse duration.

We conducted simulations to assess the performance of the deep-red mode-locked fiber laser under various net dispersion conditions, and the results are plotted in Fig. S9. The evolution of the spectrum and pulse versus the net dispersion are shown in Figures S9(a, b), respectively. Figure S9(c) depicts the spectral bandwidth and pulse duration in simulation and experiment, respectively. With net dispersion ranging from -0.098 ps^2 to +0.094 ps^2, the spectral bandwidth initially widens and subsequently narrows, while the pulse duration first decreases and then widens, closely aligning with the experimental outcomes. Therefore, to achieve the narrowest possible laser pulse duration, which corresponds to the widest mode-locked spectral bandwidth, fine-tuning the intracavity net dispersion to near-zero is imperative.

5. Experimental setup of the 2PM

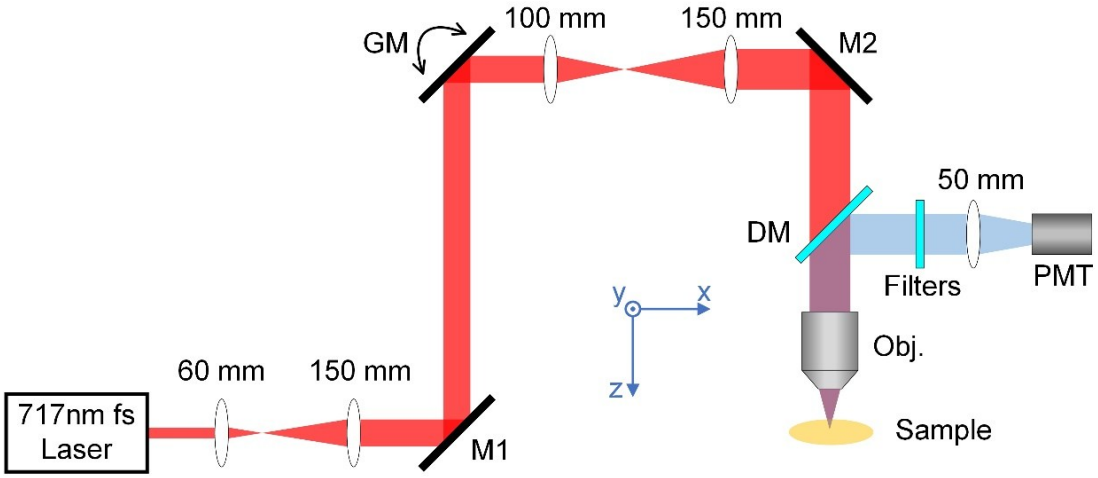

Fig. S10 Experimental setup of the 2PM system. M, mirror; GM, galvanometric scanning mirror; DM, dichroic mirror; PMT, photomultiplier tube.

The experimental setup of the 2PM is illustrated in Fig. S10. Before guiding the laser beam into the microscopy, the beam size from the laser cavity was magnified by a telescope, consisting of a pair of lenses (focal length, 60 and 150 mm), to reach the beam diameter at ~4 mm. In the 2PM, a set of *x*-*y* galvanometric scanning mirrors (GM, Sino Galvo, SG1105) was used for laser scanning. The raster-scanned light was relayed to the objective lens (Obj., Olympus LUMPLFL60XW, NA 0.9, water immersion) through a telescope, consisting of a 100-mm and a 150-mm lens, aiming to cover the back focal aperture of the objective. A longpass dichroic mirror (DM, LP650, JXOPTIX, OFD1LP-650) was placed before the objective for transmitting the excitation beam and reflecting the emission signal. The generated signal was collected in the epi direction by a 50-mm lens. The residual excitation beam was cleaned up by a shortpass filter (SP650, JCOPTIX, OFE1SP-650), while additional optical filters (SP500, BP520, and

LP590) were separately used to pick up specific signals at different wavelength bands, i.e., the 2P-excited fluorescence emitted by different dyes. The imaging signal was detected by a large-area photomultiplier tube (PMT, Hamamatsu H11901-20), limiting the movement of the signal beam on the sensor area to avoid scanning artifacts. The electrical signal from the PMT was subsequently amplified by a amplifier unit (C12419, Hamamatsu) and digitized by an analogue-to-digital converter card (National Instruments PCI-6110, 5 MS/sec). The control of the entire 2PM system was based on Matlab, including the laser scanning, data collection, and image reconstruction.

6. Sample Preparation

Mouse kidney section. The tissue is a 16-μm-thick commercial cryosection from Thermo Fisher (Catalog number, F24630), stained with Alexa Fluor 488 (AF488), Alexa Fluor 568 (AF568), and DAPI (D-1306).

Fluorecent Microspheres. The sample are 200-nm carboxylate-modified microspheres from Thermo Fisher (Catalog number, F8809). The excitation and emission wavelengths are 540 and 560 nm, respectively. The beads were used to measure the lateral resolution of the 2PM.

C.elegans. Fixation and imaging: dRIs247 [Pact-5-mCherry-HA-act-5; Cb.unc-119(+)] was grown to the L4 stage on OP50 and washed off by M9 buffer. Then they were fixed by fixing solution (4% formaldehyde) and rotated at room temperature for 0.5h. The fixed worms were washed with M9 buffer and transfer to a 2% agarose gel pad for imaging. ACT-5, a microvillus-specific actin, was located at the apical site in intestinal cells, which was a biomarker of intestinal lumen in *C. elegans*. Using transgenic strains dRIs247 [Pact-5-mCherry-HA-act-5; Cb.unc-119(+)], intestinal lumen was observed by microscope in *C.elegans*.

7. Data acquisition

The images in 2PM were collected at a 2D frame rate of ~0.2 Hz over a field of view of 120 × 120 μm^2 [Figs. 6(a, c, f)] or 60 × 60 μm^2 [Fig. 6(g)] with 512 × 512 pixels. The frame rate here is majorly limited by the speed of the galvanometric mirrors. In the imaging experiments, only the seed laser was utilized without power amplification, as the required laser power after the objective was ~12 mW.

8. 2PM resolution

In 2PM, the lateral resolution can be expressed as[34]:

$$\mathrm{FWHM_{xy}} = 2\sqrt{ln2} \times \begin{cases} \frac{0.320\lambda}{\sqrt{2}\mathrm{NA}} & \mathrm{NA} \leq 0.7 \\ \frac{0.325\lambda}{\sqrt{2}\mathrm{NA}^{0.91}} & \mathrm{NA} > 0.7 \end{cases} \quad (6)$$

where FWHM is the full width at half maximum of the PSF, NA is the effective numerical aperture of the objective lens, and λ is the wavelength of the excitation laser.